Giant monopole and quadrupole resonances and other multipole excitations in ^{208}Pb studied in 43 MeV/nucleon α-particle and deuteron scattering

H. P. Morsch, C. Sükösd, M. Rogge, P. Turek, and H. Machner
Institut für Kernphysik, Kernforschungsanlage Jülich, D-5170 Jülich, West Germany

C. Mayer-Böricke
Institut für Kernphysik, Kernforschungsanlage Jülich, D-5170 Jülich, West Germany
and Physics Department, University of Bonn, D-53 Bonn, West Germany

(Received 22 January 1980)

Inelastic excitations of ^{208}Pb up to the giant resonance region were investigated in 172 MeV α and 86 MeV d scattering. In the spectra, the giant resonance bump exhibits a double structure; the well known isoscalar giant quadrupole resonance at 10.9 ± 0.3 MeV, and the new resonance at 13.8 ± 0.3 MeV, for which evidence exists for $L = 0$. Both resonances have a full width at half maximum of 2.6 ± 0.3 MeV. Below the giant resonances two new structures were found at excitation energies of 7.4 and 8.1 MeV which were identified as hexadecapole excitations with a strength of 3 and 2.7 single particle units, respectively. Angular distributions have been obtained for high-lying excitations as well as for the low-lying 3^-, 5^-, 2^+, and 4^+ states. Microscopic distorted-wave Born-approximation calculations have been performed using double folding form factors. In this approach a good description of our scattering data has been achieved. For low-lying excitations our results are consistent with electron and proton scattering analyses. For the giant quadrupole resonance the angular distributions cannot be described assuming pure $L = 2$ excitation. Different assumptions about other contributing multipole strengths are discussed. Assuming the 13.8 MeV resonance to be the giant monopole excitation, several models yield differential cross sections which are inconsistent with the data. A consistent description of α and d scattering is obtained if, in addition to the compressional $L = 0$ mode, diffuseness effects are considered as well as other contributing multipole strength ($L = 1$). With the transition density used, the monopole strength corresponds to about 90% of the energy weighted sum rule limit. The result of a recent ^{16}O scattering experiment suggesting a pronounced $L = 3$ and 5 resonance at $E_x \simeq 20$ MeV in ^{208}Pb is not confirmed.

[NUCLEAR REACTIONS ^{208}Pb(α,α'), E_α=172 MeV, ^{208}Pb(d,d'), E_d=86 MeV, measured $\sigma(\theta)$. Deduced strength of multipole excitation up to the giant resonance region.]

I. INTRODUCTION

During the last few years the excitation of giant resonances was studied quite intensely in electron and hadron scattering.[1] In hadron scattering most of the data exist for the isoscalar giant quadrupole resonance which has been excited by light[1] and heavy ions.[2] Recently, considerable effort was made to investigate also the isoscalar giant monopole resonance, the breathing mode of the nucleus. However, in identifying the monopole strength, difficulties arise from the fact that $L=0$ and 2 angular distributions are very similar in scattering processes which yield sizable cross sections, as, e.g., in α scattering.[3] There are several ways to overcome this difficulty. The first is to study extreme forward angles[4] where large differences are expected to occur between $L=0$ and 2 excitation. This is the most direct way to identify the monopole strength, but there are large experimental difficulties related to background problems and other disturbing effects. Another possibility is to utilize dynamical properties, e.g., the study of the energy dependence[5] of the giant resonance cross section. A third and more indirect way is the consistent study of different scattering systems. However, in such a study one is more sensitive to nuclear models because monopole cross sections depend strongly on the inelastic form factor.[6]

For ^{208}Pb the first two methods have been applied[4,5] and yield evidence for the monopole character of the resonance at $E_x = 13.8$ MeV. In this study we applied the third method by measuring this resonance in α and d scattering. In both scattering systems we are restricted to isoscalar excitations. However, differences arise from the fact that due to the strong absorption in α scattering, mainly the tail of the nuclear density contributes to the cross section, whereas in d scattering larger contributions are expected from the nuclear interior. Spin-flip excitations are also possible in (d,d'); however, the corresponding cross sections are strongly reduced as compared to those

for non-spin-flip excitations.[7]

Another aspect of this study is the investigation of the different multipole contributions in the giant resonance region. From random-phase approximation (RPA) calculations appreciable strength of multipolarities different from $L=2$ is predicted,[8-10] in particular a large amount of $L=4$ strength between $8 \lesssim E_x \lesssim 12$ MeV. Further, a concentration of $L=3$ strength is expected at larger excitation energy between 16 and 20 MeV.[10] Here, it should be noted that a structure at about 20 MeV has been observed in ^{16}O scattering[11] which was interpreted as a giant $L=3$ and 5 excitation.

In analyzing our experimental data distorted-wave Born approximation (DWBA) calculations were performed using double folding form factors. In this folding approach different scattering systems can be described consistently and a direct comparison with electron scattering results is possible. For a test of this approach we studied the excitation of low-lying 3^-, 5^-, 2^+, and 4^+ states.

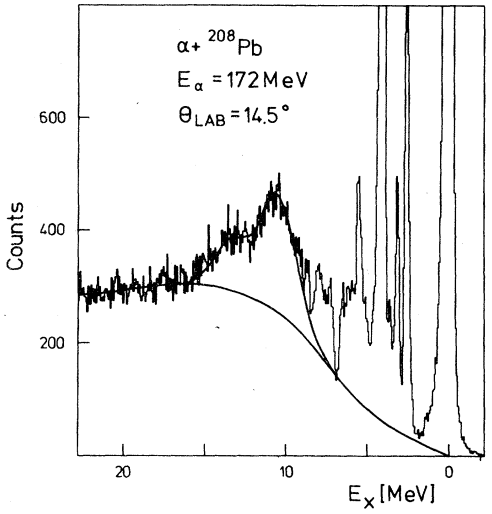

FIG. 1. Spectrum of α scattering from ^{208}Pb at 172 MeV incident energy. The background line and the double Gaussian fit to the giant resonances are discussed in the text.

II. EXPERIMENTS AND RESULTS

The experiments were performed using momentum analyzed beams of α particles and deuterons with an energy of 43 MeV/nucleon from the Jülich isochronous cyclotron JULIC. The scattered particles were detected by two counter telescopes each consisting of 2 mm silicon and 24 mm Ge-Li detectors for the ΔE and E counter, respectively. The energy resolution in the spectra was 10^{-3} full width at half maximum (FWHM). Clean ^{208}Pb targets of 5–8 mg/cm^2 were made which contained very small contamination of ^{12}C and ^{16}O.

Figures 1 and 2 show spectra of scattered α particles and deuterons obtained at scattering angles of 14.5° and 23°, respectively. In both scattering systems a double structure of the giant resonance is clearly seen. The larger peak at an excitation energy of 10.9 ± 0.3 MeV corresponds to the giant quadrupole resonance observed in other hadron and electron scattering.[1-4] The other resonance has an excitation energy of 13.8 ± 0.3 MeV. For both resonances a width (FWHM) of 2.6 ± 0.3 MeV was obtained. This is in excellent agreement with the lower energy data.[3,4] The spectra have been analyzed by fitting the giant resonance region with two Gaussian peaks superimposed on a continuous background as illustrated in Figs. 1 and 2.

In our high energy α spectra the background relative to the giant resonance peak is much smaller as compared to lower α incident energies.[5] Also a better peak to background ratio is obtained than in most other scattering systems including heavy ion scattering.[2] However, in our data analysis the largest uncertainties still are due to the uncertainty in the assumed shape of the nuclear continuum. The background shape was determined in the following way: In most spectra quite a flat continuum has been observed above the giant resonance bump (Figs. 1 and 2). This high energy background has been extended down to the low energy discrete spectrum by a smooth polynomial fit going through the minima of the discrete spectrum. In this way a consistent evaluation of spectra at all measured angles was achieved with a smooth angular depen-

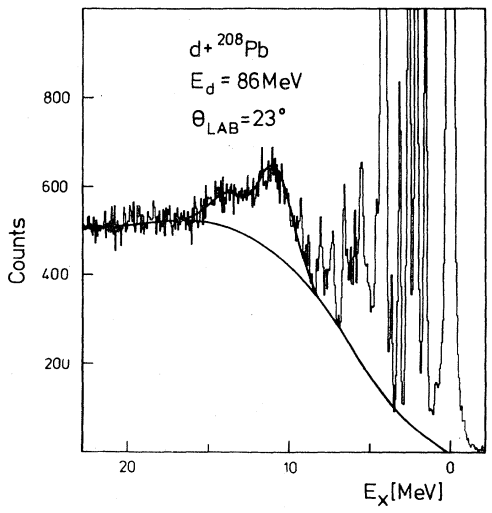

FIG. 2. Spectrum of d scattering from ^{208}Pb at 86 MeV incident energy. The background line and the fit to the resonances are indicated.

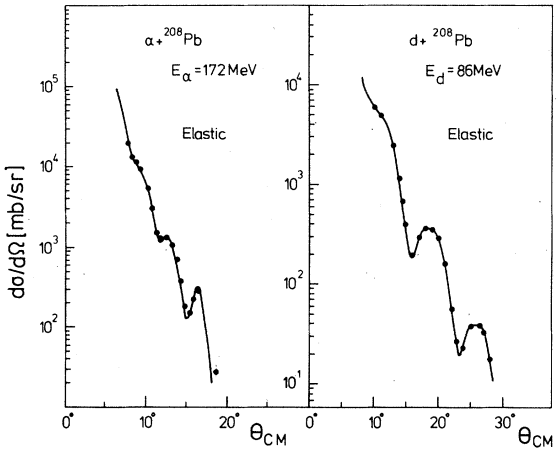

FIG. 3. Measured angular distributions of elastic α and d scattering in comparison to optical model calculations with parameters in Table I (sets 1 and 3).

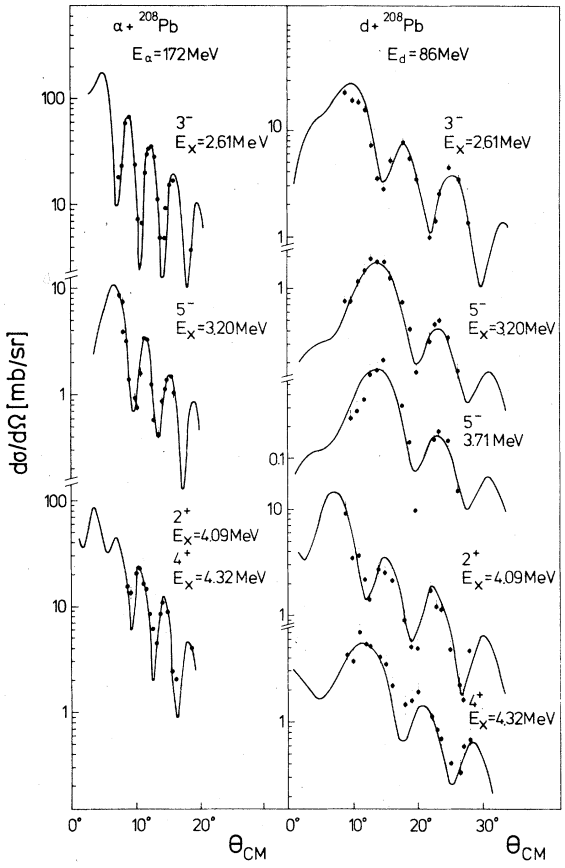

FIG. 4. Measured differential cross sections for α and d inelastic scattering to low-lying states and results of microscopic DWBA calculations. For the 2^+ and 4^+ excitation in α scattering only the sum cross section is obtained. A ratio β_4/β_2 of 1.2 was found from fitting the shape of the diffraction pattern.

dence of the background under the giant resonances. Typical uncertainties in the deduced cross section of giant resonances are ± 20% for α scattering and ±30% for d scattering, due to the significantly larger background. These errors have been estimated by using different background shapes in the excitation region 8 to 16 MeV. The background subtracted is expected to contain, in addition to contributions from precompound and other processes, broad structures of direct excitation. Such structures are predicted by microscopic RPA calculations up to quite high excitation energies.[9,10]

On the low energy shoulder of the giant quadrupole resonance (Figs. 1 and 2) there is indication for the fine structure seen in high resolution proton scattering.[12] In particular, the structure at 9.3 MeV is seen in our spectra. At lower excitation energies of 7.4 and 8.1 MeV we find two new structures for which complete angular distributions have been obtained. Further, unresolved structure was observed in the region from 5 to 7 MeV. The fact that large differences are found in the shape of this structure at different scattering angles may indicate excitations of different multipolarities. It is interesting to note that at 6.3 MeV

TABLE I. Optical potentials for α and d scattering from ^{208}Pb. $\alpha+^{208}$Pb, $E_\alpha = 172$ MeV: set 1; $d+^{208}$Pb, $E_d = 86$ MeV: sets 2–4. $r_c = 1.3$ fm.

Set	V_0 (MeV)	r_0 (fm)	a_0 (fm)	W [a] (MeV)	r_W (fm)	a_W (fm)	V_{so} (MeV)
1	155.0	1.282	0.677	23.26	1.478	0.733	
2	83.74	1.15	0.817	17.84	1.028	1.24	11.33
2a	83.74	1.15	0.817	17.84	1.028	1.24	5.67
2b	83.74	1.15	0.817	17.84	1.028	1.24	11.33 [b] 0.0
3	83.79	1.15	0.861	18.90	1.170	0.873	9.38
4	82.20	1.15	0.895	12.83	1.189	0.93	18.94

[a] Set 1: volume absorption. Sets 2–4: surface absorption.
[b] 11.33 MeV in entrance channel, no V_{so} potential in exit channel.

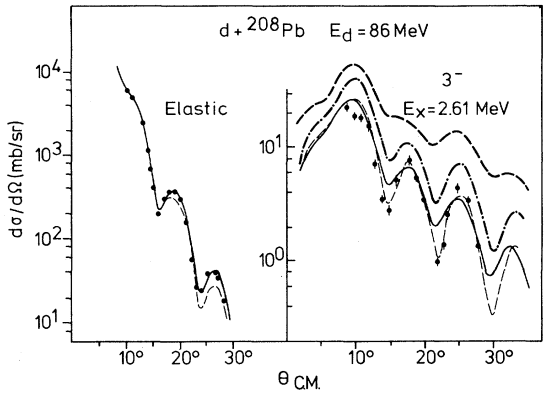

FIG. 5. Dependence of elastic and inelastic cross section in d scattering on the optical potential. Solid, dot-dashed, and thick dashed line correspond to the use of potential sets 2, 3, and 4, respectively (Table I). The thin dashed line is obtained by using potential set 2a. For inelastic cross sections the absolute normalization [Eq. (3)] was the same in all calculations.

a peak strongly excited in (d,d') is not clearly seen in the (α,α') spectra. This may indicate a spin-flip excitation, possibly of the 6.26 MeV state observed in (p,p').[12] To resolve the different structures in this region, currently high resolution experiments are being performed using the new Jülich Magnetic spectrometer BIG KARL.

Angular distributions of elastic scattering are

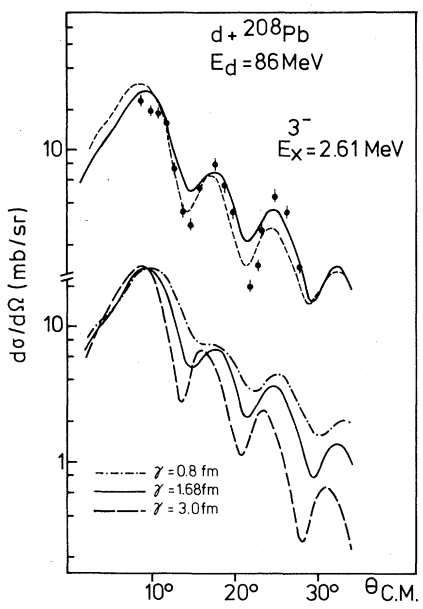

FIG. 6. Effect of using a complex form factor (upper part, dashed line) and dependence on the range of the nucleon-nucleon force (lower part) in (d,d'). The solid lines correspond to the standard calculation (with real form factor). In all calculations shown here optical potential set 2 (Table I) was used.

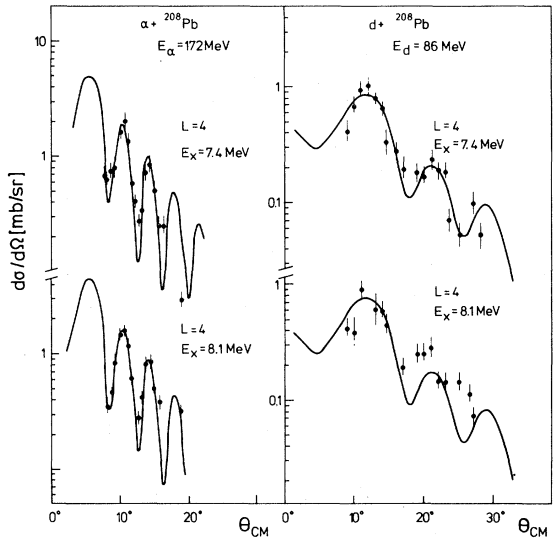

FIG. 7. Measured angular distributions for inelastic excitation of states at 7.4 and 8.1 MeV and comparison with $L = 4$ DWBA predictions.

shown in Fig. 3. Optical potentials which fit these data are given in Table I. For the low-lying excitations to 3^-, 5^-, 2^+, and 4^+ states the angular distributions are given in Fig. 4. Figures 5 and 6 show the results of different calculations for (d,d'). Differential cross sections for the exci-

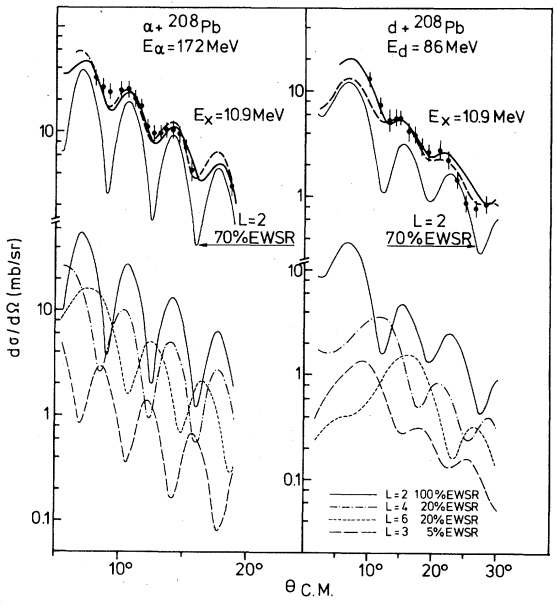

FIG. 8. Differential cross sections for the excitation of the 10.9 MeV resonance in comparison with DWBA calculations. Upper part: multipole excitation with strength parameters in Table VI (fit 1, dashed line; fit 2, thick solid line). The differential cross sections in the lower part correspond to calculations for $L = 2$ to $L = 6$ with the sum rule strengths indicated.

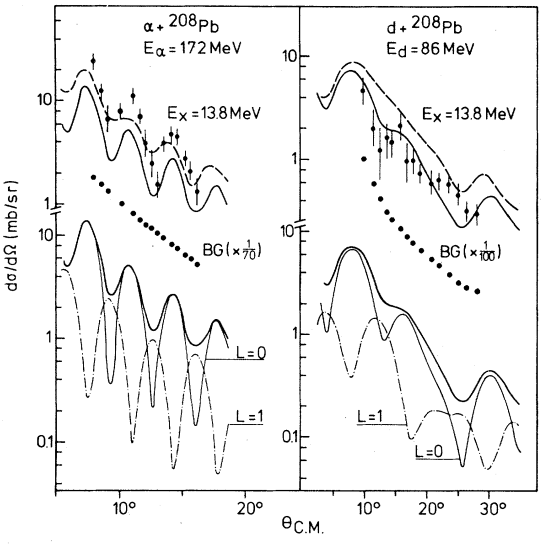

FIG. 9. Experimental cross sections for excitation of the 13.8 MeV resonance and theoretical estimates. The thin solid and dot-dashed curves in the lower part correspond to monopole excitation (using ρ_{TR1}) and dipole excitation, respectively. The sum given by the thick solid line is compared to the data in the upper part. The dashed line corresponds to a calculation in which in addition to $L=0$ and 1 excitation also $L=4$ and $L=6$ contributions are assumed as discussed in the text. The full points shown without error bars indicate the cross section of the background (BG) subtracted under the 13.8 MeV resonance (see Figs. 1 and 2).

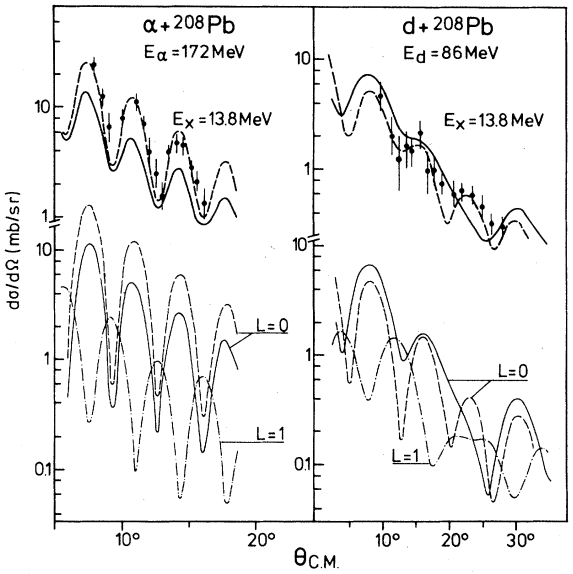

FIG. 10. Differential cross section for the 13.8 MeV resonance excited in α and d scattering in comparison with calculated cross sections using the monopole transition density ρ_{TR3} (thin dashed lines). The sum of this $L=0$ and of the $L=1$ excitation (dot-dashed lines) is given by the thick dashed lines in the upper part of the figure. For comparison also the results of Fig. 9 are shown: the sum of $L=0$ contributions using ρ_{TR1} (thin solid lines) and $L=1$ contributions (dot- dashed lines) is given by the thick solid lines shown in the upper part of the figure. In all cases optical model potential sets 1 and 2b (Table I) have been used.

tations at 7.4 and 8.1 MeV are given in Fig. 7 and those for giant resonance excitations in Figs. 8 and 9. In Fig. 9 differential cross sections of the underlying background are shown for the 13.8 MeV resonances also. Quite similar is the angular dependence of the background for the 10.9 MeV resonance but with an absolute cross section smaller by about 10%. The error bars in Figs. 4–10 are due to uncertainties in the background subtraction in addition to statistical errors and uncertainties from subtracting contaminant lines. In Figs. 8 and 9 the typical error of ±20% for α and ±30% for d scattering is shown if not indicated otherwise.

III. MICROSCOPIC CALCULATIONS AND DESCRIPTION OF LOW-LYING EXCITATIONS

In order to find a consistent description of our inelastic α and d scattering data we performed DWBA calculations using foldinglike form factors.[6,12–14] In the following formulas and definitions are given and transition densities for different excitations are discussed. Then this method is applied to the analysis of the inelastic data concerning low-lying excitated states. The reason for this is to test the microscopic approach and to adjust the strength of the effective nucleon-nucleon force needed for the description of the investigated scattering systems. The parameters adjusted in this way will then be used in Sec. IV without further modifications to analyze the data of higher excited states.

The inelastic form factor is given by[14]

$$F(R) = (4\pi)^2 \int\int \rho_{TR}(r)\rho_{proj}(r') \times v(|\vec{R}+\vec{r}-\vec{r}'|)r^2 dr\, r'^2 dr' \quad (1)$$

and the matrix element of the r^L operator by

$$\langle r^L \rangle = 4\pi \int \rho_{TR}(r) r^{L+2} dr , \quad (2)$$

where $\rho_{TR}(r)$ is the target transition density, $\rho_{proj}(r')$ is the projectile density, and $v(|\vec{R}+\vec{r}-\vec{r}'|)$ is the normalized effective nucleon-nucleon interaction acting between the nucleons of the target and those of the projectile; R is the distance between target and projectile centers of mass. For the effective interaction a real Gaussian shape with a range of 1.68 fm was used. This interaction,[15] with a volume integral of 446 MeV fm^3, has been applied succesfully to different scattering

systems[6,12,13] and yields a quantitative description of low-lying states in ^{208}Pb excited in 48 MeV α scattering.[16] Except for $L=0$ and $L=1$ excitations which are discussed below, simple surface-derivative-type transition densities $\rho_{TR} \sim [d\rho(r)]/dr$ were used, $\rho(r)$ being the ground state density with parameters of Ref. 17.

For the low-lying excitations in Fig. 4 we used a simple relation[18] between proton and neutron transition densities $\rho^p_{TR}(r) = (Z/N)\rho^n_{TR}(r)$. By this the inelastic cross section $d\sigma/d\Omega$ is directly connected[14,18] to the electromagnetic transition strength $[B(\mathrm{EL}) = (2L+1)Z^2/A^2|\langle r^L\rangle|^2]$:

$$\frac{d\sigma}{d\Omega} = \left(\frac{d\sigma}{d\Omega}\right)_{DW} \left| 4\pi n V \frac{A}{Z} \frac{1}{\langle r^L\rangle} \right|^2 B(\mathrm{EL}) . \tag{3}$$

$[(d\sigma)/(d\Omega)]_{DW}$ is the DWBA cross section[19] obtained using the microscopic form factor of Eq. (1). The number of projectile nucleons is denoted by n. The strength of the nucleon-nucleon interaction V is adjusted to fit the data of the low-lying excitations (Fig. 4).

For high-lying isoscalar excitations the inelastic strength will be compared to the corresponding energy weighted sum rule (EWSR) (Ref. 20)

$$S(L) = \sum_c |\langle r^L\rangle|^2 E_c ;$$

c sums over all proton and neutron components with multipolarity L. It is given for $L=0$ by[20]

$$S(L=0) = \frac{2\hbar^2}{m} A \langle r^2\rangle_{g.s.} \tag{4}$$

and for $L \geq 2$ by

$$S(L) = L(2L+1)^2 \frac{\hbar^2}{8m\pi} A \langle r^{2L-2}\rangle_{g.s.} . \tag{5}$$

For $L>2$ we used[21] the approximation $\langle r^{2L-2}\rangle_{g.s.} = 3(2L+1)^{-1} R_0^{(2L-2)}$ with $R_0 = 1.2 \cdot A^{1/3}$ fm. Since the summation is over proton and neutron components, the EWSR is adequate for isoscalar excitation in hadron scattering. The corresponding electromagnetic sum rules[20] are smaller by a factor of Z^2/A^2. Quite similar to Eq. (3), the inelastic cross section is related to the EWSR strength for $L=0$ by

$$\frac{d\sigma}{d\Omega} = \left(\frac{d\sigma}{d\Omega}\right)_{DW} 4\pi \left| nV \frac{1}{\langle r^2\rangle} \right|^2 \frac{S(L=0)}{E_x} \tag{6}$$

and for $L \geq 2$ by

$$\frac{d\sigma}{d\Omega} = \left(\frac{d\sigma}{d\Omega}\right)_{DW} \left| 4\pi n V \frac{1}{\langle r^L\rangle} \right|^2 \frac{S(L)}{E_x} . \tag{7}$$

For a monopole transition the form of ρ_{TR} is quite different from a surface derivative. This is due to the constraint $\int \rho_{TR} d\tau = 0$ giving rise to a different sign of ρ_{TR} in different radial regions. We applied different models for $L=0$: the Tassie model[22] with

$$\rho_{TR1} = 3\rho(r) + r\frac{d\rho(r)}{dr} ,$$

a microscopic 1p1h description (ρ_{TR2}) as in Ref. 12, and a collective model using ρ_{TR3} in form of a derivative of the ground state density.[23]

The comparison of these different monopole transition densities (normalized to 90% EWSR strength) shows a rather close agreement of ρ_{TR1} and ρ_{TR2}. Also the collective density[23] is quite similar if only a compressional mode is assumed. However, in this model[23] a vibration of the nuclear surface (diffuseness oscillation) is also possible and the corresponding transition density is very different from that of the compressional mode. It will be discussed in more detail in Sec. IV C.

In addition to the multipole excitations discussed above, there may be a certain amount of dipole excitation of the giant dipole resonance, centered at $E_x = 13.4$ MeV (Ref. 24) in ^{208}Pb. The isoscalar component of this mode can be excited in nuclei with $N>Z$ by isoscalar projectiles such as α particles and deuterons. In a simple approximation the dipole transition density may be estimated as follows: For the excitation of the $T_<$ component of the 1^-, $T=1$ excitation, isovector and isoscalar transition densities are given by $\rho^{T=1}_{TR} = \rho^p_{TR} + \rho^n_{TR}$ and $\rho^{T=0}_{TR} = \rho^p_{TR} - \rho^n_{TR}$. Except for Coulomb excitation at extremely small angles, α particles and deuterons excite only the $T=0$ component. By using for the outside region $\rho_{TR} \sim d\rho(r)/dr$ and $\rho^p_{TR} = Z/N \cdot \rho^n_{TR}$, we obtain

$$\rho^{T=0}_{TR} \sim (Z-N)\frac{d\rho(r)}{dr} . \tag{8}$$

The dipole cross section is given by[25]

$$\frac{d\sigma}{d\Omega} = \left(\frac{d\sigma}{d\Omega}\right)_{DW} \left| 4\pi n V \frac{(Z-N)}{A \cdot \langle r\rangle} \right|^2 \frac{S(L=1)}{E_x} , \tag{9}$$

where the energy weighted dipole sum rule[20] is given by

$$S(L=1) = \frac{9\hbar^2}{8\pi m} \frac{N \cdot Z}{A} . \tag{10}$$

The use of approximation (8) is good only for a purely peripheral reaction and should be applicable for α scattering. In a more correct treatment the $T=0$ transition density has to be corrected for spurious center of mass motion. This is discussed in Ref. 25 using a similar collective description as in Ref. 23. The cross section so obtained is very similar to that estimated by approximation (8) for α scattering. For d scattering larger differences are obtained. The dipole cross

sections shown in Figs. 9 and 10 are those of the more accurate calculations in Ref. 25 assuming a dipole strength of 75% of the $E1$ EWSR. This is in agreement with experimental $E1$ strengths found in the energy region[24] of the giant monopole resonance.

In the following the description of low-lying excitations (Fig. 4) is discussed. In Eq. (3) the differential cross section scales with the electromagnetic transition strength; however, it is also dependent on the radial extent of the transition density. We made an attempt to test the quality of the used surface derivative transition densities by comparing transition radii $(\langle r^{L+2}\rangle/\langle r^L\rangle)^{1/2}$ for the different transition with results from electron scattering. In Table II transition radii obtained from our simple transition density $d\rho(r)/dr$ are compared to those from the electron scattering analysis of Ref. 26. Although in Ref. 26 a different form $\rho_{TR}(r) \sim r^{L-1} \times d\rho(r)/dr$ is used [however, with the geometry parameters of $\rho(r)$ adjusted to describe the cross sections for each state separately], the resulting transition radii (Table II) are in remarkable agreement with those of the simple surface derivative (with fixed geometry in Ref. 17). This indicates that the used form of the transition density $d\rho(r)/dr$ is adequate for our analysis. In the case of the 3^- state we performed also calculations using the transition density of Ref. 26. We found that the cross sections so obtained are very similar to those obtained by using the surface derivativelike transition density. Also by using the RPA wave functions of Ring and Speth[8] good agreement with the data in Fig. 4 is obtained.

Optical potentials used to calculate the DWBA scattering amplitudes are those in Table I. For inelastic α scattering the calculated cross sections are not very sensitive to small changes in the optical potentials; the measured angular distributions of low-lying states in Fig. 4 are well described. In d scattering we have quite a different situation: The DWBA cross sections are very sensitive to the deuteron optical potential. This is shown in Fig. 5. DWBA cross sections for the lowest 3^- excitation are given using different optical potentials which all fit elastic scattering (the same normalization of the calculated cross sections is used for the different calculations). Both absolute height and structure are quite different; moreover, in three cases the structure of the angular distribution was less pronounced than that of the experimental data. It was not possible to find an optical potential which could describe consistently elastic and inelastic scattering in the usual way.

To overcome these difficulties in the DWBA description of d scattering one may use modified optical potentials, e.g., in the outgoing channel. Another possibility is the use of a changed effective force in the inelastic form factor [Eq. (1)]; this will be discussed below. As shown by the thin dashed line in Fig. 5, a better description of the deep diffraction structures in the inelastic cross section can be obtained by reducing the depth of the spin-orbit potential to $V_{so}=5.67$ MeV. However, by this (potential set 2a in Table I) the elastic scattering is not fitted well any longer (thin dashed line in Fig. 5). If for the entrance channel the optical potential (set 2 in Table I) is not changed, thus keeping the good fit to the elastic data in Fig. 5, then a good description of inelastic scattering is obtained by using $V_{so} \sim 0$ MeV for the outgoing channel (set 2b in Table I). The fit is very similar to that obtained by using $V_{so}=5.67$ MeV for in and outgoing channels (thin dashed line in Fig. 5). Using these modifications a good description of the (d, d') angular distributions of all low-lying excitations is obtained (see Fig. 4). It should be noted that the changes made in the spin-orbit potential may not be unique. It could well be that other changes in the optical potential have similar effects on the inelastic cross section.

In Table III B(EL) values deduced from our inelastic cross sections by the relation (3) are compared to those obtained from electron scattering[26] and lower energy α scattering[16] results. If for the 172 MeV α scattering data the strength of the effective interaction $V=16.92$ MeV (yielding a volume integral of 446 MeV fm^3) was increased by 20%, a

TABLE II. Transition radii (fm) for $\rho_{TR}=d\rho(r)/dr$ [$\rho(r)$ ground state WS density with parameters in Ref. 17] in comparison with (e, e') results of Ref. 26.

J^π	E_x (MeV)	$d\rho(r)/dr$	(e, e')
3^-	2.61	7.4	7.7
5^-	3.20	7.8	8.0
2^+	4.09	7.2	7.2
4^+	4.32	7.6	7.4
6^+	4.43	7.9	7.8

TABLE III. B(EL) values (e^2 fm^{2L}) extracted from our data in comparison with (e, e') results of Ref. 26 and 48 MeV α scattering (Ref. 16).

J^π	E_x (MeV)	(d, d') 86 MeV	(α, α') 172 MeV	(α, α') 48 MeV	(e, e')
3^-	2.61	7.74×10^5	7.74×10^5	7.70×10^5	7.72×10^5
5^-	3.20	5.48×10^8	5.64×10^8	5.73×10^8	4.51×10^8
5^-	3.71	1.38×10^8		2.26×10^8	3.25×10^8
2^+	4.09	3.50×10^3	3.70×10^3	2.94×10^3	2.96×10^3
4^+	4.32	1.66×10^7	1.60×10^7	1.25×10^7	1.29×10^7

good agreement with (e,e') results was achieved (Table III). To arrive at the same good agreement of the inelastic strengths for (d,d') (Table III) no renormalization of the force was needed. Only in the case of the second 5^- state at 3.71 MeV the extracted strength from the high energy (d,d') data does not quite agree with those extracted from the lower energy (α,α') and the (e,e') data. This could indicate that the transition density for this rather weak transition is quite different from the simple surface derivative used; this is supported by microscopic calculations[10] which yield a node in the transition density.

For completeness we have compared our results also with the result of (p,p') (Ref. 27) obtained at a proton energy of 61.2 MeV. Here it is better to compare directly deformation parameters which are given by $\beta_L = [(4\pi)/(3ZR^L)][B(\mathrm{EL})]^{1/2}$. R is here the radius of the projectile-nucleus potential which is either taken from the optical potential or from a folded potential. For the results given in Table IV, R was used from the α optical potential. Good agreement is obtained again except for the second 5^- state. We conclude that the present approach yields an excellent description of our data on low-lying excitated states in (d,d') and (α,α') scattering with strengths which are consistent with (e,e'), (p,p') and lower energy α scattering.

We tried still other ways to modify the DWBA description for the (d,d') data by using a different inelastic form factor. In this case the optical potentials used for the calculation of the differential cross sections were kept unchanged. First, we have performed calculations using a complex form factor (see Ref. 28). We applied the usual method by taking for the imaginary part of the form factor the derivative of the imaginary optical potential. The result for the 3^- excitation is shown by the dashed line in the upper part of Fig. 6. For the deformation parameter of the imaginary part a value of $\beta_3^{\mathrm{im}} = 0.13$ was used. As compared to the standard calculation (solid line) an improvement is obtained in the depth of the diffraction minima (dashed line, upper part in Fig. 6). In particular, the first minimum at 15° is well fitted. However, the quality of fit for the whole angular distribution is not improved.

Further it was tested whether a modified range of the effective interaction in Eq. (1) would yield a consistent description of elastic and inelastic data. Consequently, we performed additional calculations using a rather short range of 0.8 fm and a long range of 3 fm. These results are also shown in Fig. 6 (lower part). Clearly, the structure in differential cross sections is sensitive to the range of the force. For larger effective ranges deeper structure is obtained which is more consistent with the data. However, the position of the maxima and minima is shifted to smaller angles as compared to the data and the general slope is too steep. Therefore, by also making these modifications no satisfactory description of the (d,d') data is obtained.

Finally, it should be noted that the problems in the description of (d,d') discussed above are less important for high-lying giant resonance excitations. For these the structure in the differential cross section is less pronounced and also not so sensitive to the optical potential. Angular distributions for excitation of the giant quadrupole resonance are, e.g., quite similar if potential sets 2, 2a, or 2b are used. Thus, regardless of the difficulties in the description of low-lying excitations, the used DWBA method should be reliable for the description of high-lying excitations.

TABLE IV. Deformation parameters β_L from our (α,α') results in comparison with (p,p') results of Ref. 27.

J	E_x (MeV)	(α,α') present results	(p,p') Ref. 27
3^-	2.61	0.103	0.103
5^-	3.20	0.048	0.044
5^-	3.71	0.024	0.032
2^+	4.09	0.053	0.055
4^+	4.32	0.063	0.064

IV. DISCUSSION OF HIGH-LYING EXCITATIONS

The spectra in Figs. 1 and 2 indicate a rich structure of excitations in ^{208}Pb up to the giant resonance region. In the following we discuss four subjects: new hexadecapole structure observed at $E_x = 7.4$ and 8.1 MeV, the giant quadrupole resonance at $E_x = 10.9$ MeV, the giant monopole resonance at $E_x = 13.8$ MeV, and finally possible giant resonance structures at higher excitation energies.

A. Hexadecapole structures at $E_x = 7.4$ and 8.1 MeV

In the spectra of α particles as well as deuterons, two well separated structures were observed at excitation energies of 7.4 and 8.1 MeV. The corresponding angular distributions are given in Fig. 7. In α scattering we observe a strong diffraction pattern similar to that observed for low-lying excitations (Fig. 4). The structure in the diffraction pattern which is sensitive to the L transfer indicates hexadecapole excitations (solid lines in Fig. 7). In (d,d') the main characteristic is a broad maximum at about 12°. This can be described only by assuming $L=4$ excitation. The strengths of these excitations derived from α and

TABLE V. Isoscalar energy weighted sum rule strengths (%) for high-lying hexadecapole excitations from (α, α') and (d, d').

E_x (MeV)	(d, d')	(α, α')
7.4	2.7	2.7
8.1	2.6	2.5

d scattering are given in Table V. They are in excellent agreement, supporting the L assignment obtained from the angular distributions. The inelastic strengths of 3.2 and 2.7 single particle units for the excitation of the 7.4 MeV and the 8.1 MeV states, respectively, may indicate collective excitations. Together with the low-lying 4^+ excitation at $E_x = 4.32$ MeV, a total hexadecapole strength of 15% of the isoscalar EWSR is observed. Larger $L = 4$ strength is predicted[8-10] at higher excitations, in particular in the region of the giant quadrupole resonance. This is discussed below.

B. The giant quadrupole excitation at $E_x = 10.9$ MeV

The largest bump occurs in the spectra at $E_x = 10.9$ MeV (Figs. 1 and 2). It corresponds to the giant quadrupole resonance observed in different scattering systems.[1-5] Angular distributions are given in Fig. 8. They are rather featureless, in contrast to those at lower excitations (Figs. 4 and 7). A comparison was made with a pure quadrupole DWBA calculation (upper thin solid line in Fig. 8) which shows deep structure. A fit to the experimental distributions could be obtained only by assuming excitations of mixed multipolarity. In particular, to fill in the deep diffraction minima for $L = 2$ in α scattering, one has to assume L contributions which yield large cross sections at angles of 9, 13, and 16°; these are L values of 3 and/or 6. The need for additional contributions of L transfer different from 2 is consistent with RPA predictions[8-10] which indicate higher multipolarities in the region of the giant quadrupole resonance, e.g., a larger amount of $L = 4$ strength. Guided by the RPA predictions we tried to fit the data by assuming $L = 2$, 3, 4, and 6 contributions. The result of this fit (fit 1 in Table VI) is quite satisfactory except at scattering angles <13° in the case of (d, d') (upper dashed lines in Fig. 8). The strengths extracted are in rather good agreement with the RPA predictions in Ref. 10 (Table VI). In another calculation we included only $L = 2$, 3, and 4 excitations. The results (fit 2 in Table VI) also yield a good description of the experimental data of both α and d scattering (thick solid line in Fig. 8) except for the large angle data in d scattering. A rather large $L = 3$ strength is found,

TABLE VI. Energy weighted sum rule strengths (%) of different L transfers from the fits to the 10.9 MeV resonance in Fig. 8.

	$L = 2$	$L = 3$	$L = 4$	$L = 6$
RPA result Ref. 10	65	5	26	16
Fit 1	59	5	16	16
Fit 2	74	25	5	

which is in qualitative agreement with (p, p') results.[12] Unfortunately, because of the little structure in the experimental data it is not possible to distinguish between the two sets of multipole strength parameters in Table VI. Therefore, we cannot say that the RPA result[10] is the only way to describe the experiment. It is interesting to note that the contributions of various multipolarities are quite different in α and d scattering (see the curves in the lower part of Fig. 8 which represent the differential cross section for the EWSR strength given); e.g., $L = 6$ contributes significantly only to the maximum at 16° in (d, d'), while in (α, α') possible $L = 6$ contributions cover the whole angular range. Finally, it should be noted that both sets of multipole parameters in Table VI yield a good description of the energy dependence studied in Ref. 5.

C. The giant monopole excitation at $E_x = 13.8$ MeV

The giant monopole resonance at $E_x = 13.8$ MeV (Figs. 1 and 2) is of large current interest.[3-5] The angular distributions are given in Fig. 9. The absolute cross section found for α scattering is quite large; for most angles it is about one half of that for the 10.9 MeV excitation. This ratio is much less for (d, d'), mostly less than $\frac{1}{3}$. This finding is quite different from earlier estimates (see Ref. 29) in which the relative strength of the monopole was larger in (d, d') as compared to (α, α'). For α scattering a more pronounced diffraction pattern is observed than for the giant quadrupole resonance (this has already been observed in Ref. 3).

Differential cross sections for $L = 0$ excitation obtained by using the monopole transition densities ρ_{TR1} and ρ_{TR2} underestimate the experimental data for α scattering by roughly a factor of 2 (assuming 90% EWSR). For the maximum at 11° in the (α, α') angular distribution the Tassie density ρ_{TR1} yields 5 mb/sr (thin solid line in the lower part of Fig. 9) whereas ρ_{TR2} gives 4.5 mb/sr. Also, the RPA density of Wambach *et al.*[9] yields a too small cross section of 6 mb/sr. The shape of the $L = 0$ angular distributions was quite similar for the different types of ρ_{TR}. The thick solid

line in the lower part of Fig. 9 shows the summed differential DWBA cross sections of the $L=0$ excitation (90% EWSR using ρ_{TR1}) and of the isoscalar component of the $L=1$ excitation (75% EWSR). It is compared in the upper part of Fig. 9 with the data. This applies in the same way for the (d,d') case.

In contrast to (α,α') the (d,d') absolute cross section is better reproduced (thick solid line in Fig. 9). A deep minimum is obtained in the $L=0$ calculation at 26° which is not seen experimentally. For $L=0$, all transition densities discussed for (α,α') yield results for (d,d') which are quite similar. The more smooth structure experimentally observed is obtained in the calculation by taking into account the $L=1$ contribution, which is in this case especially important.

Although the addition of dipole excitation yields a better description of the data for (d,d'), the cross sections for α scattering are still too low. From the RPA results[9,10] we expect in the energy region of the monopole giant resonance $L=4$ and $L=6$ strengths of 3.5 and 6% of the EWSR, respectively. By adding the corresponding contributions to our theoretical cross section we obtained the dashed lines in Fig. 9 and thus larger absolute cross sections in α scattering. However, by these contributions the calculated angular distributions are smeared out (see dashed lines) and the cross sections for (d,d') are clearly too large compared to the data. Furthermore, an energy dependence (studied in Ref. 5) is obtained which is weaker than that observed experimentally.[5] We conclude that with the models applied so far we were not able to obtain a consistent description of the experimental data in Fig. 9. This result is at variance with those obtained for the other excitations for which a consistent theoretical description of (α,α') and (d,d') results was obtained (Secs. III, IV A, and IV B).

Most likely, this problem is related to the description of the monopole excitation. It is known[6] that monopole cross sections are strongly dependent on details of the inelastic form factor, specifically on the choice of the effective interaction and the transition density. First we attempted to remove the discrepancies with the microscopic calculation by introducing a density dependent interaction. We found, however, that this yields monopole cross sections for α scattering which are still far too small. They are enlarged by not more than 15%.

Larger effects can be obtained by modifying the monopole transition density. In the models discussed so far the giant monopole resonance is described entirely by the compressional mode. However, in the collective model of Ref. 23 a monopole surface mode (diffuseness oscillation) also exists which could mix to some extent with the density mode. The transition density of this surface mode is very different from that of the compression mode.[23] We performed calculations including a surface component. By varying the amplitude of the surface component a larger monopole cross section for α scattering could be obtained (without changing the EWSR strength). A good description of both α and d scattering data in Fig. 10 (thick dashed lines) is obtained by using[23]

$$\rho_{TR3}=\frac{\delta\rho_0}{\rho_0}\frac{\partial\rho(r)}{\partial\rho_0}+\frac{\delta a}{a}\frac{\partial\rho(r)}{\partial a}+\frac{\delta R}{R}\frac{\partial\rho(r)}{\partial R}+(\text{H.o.})$$

with

$$\frac{\delta\rho_0}{\rho_0}=0.02,$$

$$\frac{\delta a}{a}=-0.12,$$

and

$$\frac{\partial R}{R}=-0.005,$$

yielding 90% EWSR strength. This ρ_{TR3} leads to monopole cross sections shown by the thin dashed lines in Fig. 10; these should be compared to the thin solid lines obtained by using the Tassie model. Adding the $L=1$ contribution as discussed above (Fig. 9) yields a good fit to the data (thick dashed lines); also a good description of the measured energy dependence, reported in Ref. 5, is obtained. It should be mentioned that by using slightly different parameters for ρ_{TR3} the experimental data can be fitted also, assuming the total sum rule strength.

The use of a surface component appears to be quite sensible from a liquid drop picture of monopole vibration. If only the density vibrates then a change of the central nuclear density $\delta\rho_0/\rho_0$ of 5.3% is needed to obtain the EWSR strength of 90%. Adding a diffuseness component as discussed above results in a smaller $\delta\rho_0/\rho_0$ of 2% as used above. This could be energetically favored. A detailed discussion of diffuseness effects will be presented elsewhere.[30]

Finally, it should be noted that the inclusion of the surface mode gives rise to an interesting effect, namely an increase of the (α,α') excitation but a generally smaller cross section in (d,d') as compared to the results obtained with ρ_{TR1}. This is seen by comparing the thick dashed lines and the thick solid lines in the upper part of Fig. 10. This effect arises from the particular form of the monopole transition density (which has oppo-

site sign in different radial regions with a node at about 6 fm) and from differences in the absorption of the two scattering systems. Using optical potential sets 1 and 2a (Table I) for α and d scattering, respectively, cutoff calculations indicate that the (α,α') cross section is not sensitive to contributions at distances smaller than 8 fm whereas the monopole cross section in (d,d') is still effected at radii as small as 3 fm. A surface mode which pushes out the form factor to larger radii yields a larger transition density in the sensitive outside region for α scattering and thus larger cross sections. In (d,d'), however, there is cancellation from opposite inside and outside contributions. An additional surface term shifts the node to a larger radius of about 6.3 fm; this results in a stronger cancellation effect and thus a decreased (d,d') cross section. This decrease, which is opposite to the situation in α scattering, demonstrates the sensitivity of monopole cross sections to the particular properties of the scattering systems in question.

D. Possible structures of higher multipolarity up to $E_x \sim 20$ MeV

Guided from macroscopic as well as microscopic models of nuclear excitations one could expect giant resonance excitations of higher multipolarity, e.g., a giant octupole or hexadecapole resonance at higher excitation energies. Specifically, recent microscopic RPA results[9,10] predict a giant octupole resonance at $E_x = 18$ MeV. In a recent ^{16}O scattering experiment[11] a pronounced structure has been observed at about 20 MeV of excitation with a width somewhat larger than that found for the giant quadrupole resonance. The experimental cross section which was comparable to that of the giant quadrupole excitation was interpreted by the authors by assuming $L=3$ and $L=5$ strengths of 100% and 10–20% EWSR strength, respectively. In order to see if these results are in agreement with our spectra we calculated differential cross sections similar to those in Fig. 8. We find that already a $L=3$ excitation (with 100% EWSR strength at $E_x = 20$ MeV) yields a cross section of more than 10 mb/sr at 12° in (α,α') and at 10° in (d,d'). This is comparable to the cross sections for the giant quadrupole excitation. If the multipolarity of this resonance would be larger, e.g., $L=4$, then even larger cross sections of 20 mb/sr at 11° in (α,α') and of 16 mb/sr at 12° in (d,d') are estimated for 100% EWSR strength. On the basis of most of our spectra (e.g., Figs. 1 and 2) we cannot confirm the existence of such higher multipole resonances around $E_x \sim 20$ MeV.

V. SUMMARY

We have presented experimental cross sections for low-lying excitations and giant resonances in ^{208}Pb as obtained from inelastic α and d scattering. Angular distributions which are pronounced determine quite unambiguously the multipolarity of the transition; by this we have identified new hexadecapole structures around 8 MeV excitation energy. Giant resonances with multipolarities $L=0$, 1, and 2 were studied which are excited with quite different cross sections in (α,α') and (d,d') scattering. For the monopole excitation the cross section is sensitive to the transition density; the inclusion of a diffuseness oscillation gave a good description of the data. The differences in the monopole excitation in α and d scattering can be explained by assuming purely peripheral collision in α scattering and larger contributions from the nuclear interior in d scattering. The fact that a consistent description is obtained for both α and d scattering can be taken as further evidence for the giant monopole resonance located at $E_x \sim 80\, A^{-1/3}$ MeV.

We want to express our thanks to our theoretical group for many stimulating and helpful discussions, especially to Professor J. Speth and Dr. J. Wambach.

[1] M. Sasao and Y. Torizuka, Phys. Rev. C 15, 217 (1977) and references therein; F. E. Bertrand, Annu. Rev. Nucl. Sci. 26, 457 (1976); C. Mayer-Böricke, Nukleonika 22, 1131 (1977).

[2] H. J. Gils, H. Rebel, J. Buschmann, and H. Klewe-Nebenius, Phys. Lett. 68B, 427 (1977); M. Buenerd, D. Lebrun, J. Chauvin, Y. Gaillard, J. M. Loiseaux, P. Martin, G. Perrin, and P. de Saintignon, Phys. Rev. Lett. 40, 1482 (1978); R. Kamermans, J. v. Driel, H. P. Morsch, J. Wilczynski, and A. v. d. Woude, Phys. Lett. 82B, 221 (1979).

[3] M. N. Harakeh, K. v. d. Borg, T. Ishimatsu, H. P. Morsch, A. v. d. Woude, and F. E. Bertrand, Phys. Rev. Lett. 38, 676 (1977).

[4] D. H. Youngblood, C. M. Rozsa, J. M. Moss, D. R. Brown, and J. D. Bronson, Phys. Rev. Lett. 39, 1188 (1977); M. Buenerd, C. Bonhomme, D. Lebrun, P. Martin, J. Chauvin, G. Duhamel, G. Perrin, and P. de Saintignon, Phys. Lett. 84B, 305 (1979); N. Marty, A. Willis, M. Morlet, R. Frascaria, V. Comparat, and P. Kitching, *Proceedings of the EPS Topical Conference on Large Amplitude Collective Nuclear Motions*, edited by A. Kiss, F. Nêmeth, and F. Zimányi (MTA-KFKI, Budapest, 1979).

[5] H. P. Morsch, M. Rogge, P. Turek, C. Sükösd, and C. Mayer-Böricke, Phys. Rev. C 20, 1600 (1979).

[6] H. P. Morsch, D. Dehnhard, and T. K. Li, Phys. Rev. Lett. 34, 1527 (1975); 35, 192 (1975).

[7]S. M. Austin, in *The Two-body Force in Nuclei*, edited by S. M. Austin and G. M. Crawley (Plenum, New York, 1972), p. 285 and references therein.
[8]P. Ring and J. Speth, Nucl. Phys. A235, 315 (1974).
[9]J. Wambach, V. A. Madsen, G. A. Rinker, and J. Speth, Phys. Rev. Lett. 39, 1443 (1977).
[10]J. Wambach, thesis, Kernforschungsanlage Jülich 1979 (unpublished); J. Speth and J. Wambach, private communication.
[11]P. Doll, D. L. Hendrie, J. Mahoney, A. Menchaca-Rocha, D. K. Scott, T. J. M. Symons, K. van Bibber, Y. P. Viyogi, and H. Wieman, Phys. Rev. Lett. 42, 366 (1979).
[12]H. P. Morsch, P. Decowski, and W. Benenson, Nucl. Phys. A297, 317 (1978); Phys. Rev. Lett. 37, 263 (1976).
[13]H. P. Morsch, D. A. Lewis, and J. F. Petersen, Phys. Lett. 61B, 213 (1976).
[14]R. Kamermans, H. P. Morsch, R. de Meijer, and J. v. Driel, Nucl. Phys. A314, 37 (1979).
[15]I. Reichstein and Y. C. Tang, Nucl. Phys. A139, 144 (1969).
[16]P. Decowski and H. P. Morsch (unpublished).
[17]C. W. Jager, H. de Vries, and C. de Vries, Nucl. Data Tables 14, 479 (1974).
[18]A. M. Bernstein, Adv. Nucl. Phys. 3, 325 (1969).
[19]P. D. Kunz, distorted-wave program DWUCK (unpublished).
[20]A. M. Lane, *Nuclear Theory* (Benjamin, New York, 1965).
[21]E. C. Halbert, J. B. McGrory, G. R. Satchler, and J. Speth, Nucl. Phys. A245, 189 (1975).
[22]L. J. Tassie, Aust. J. Phys. 9, 407 (1956).
[23]H. P. Morsch and P. Decowski, Phys. Lett. 82B, 1 (1979).
[24]A. Veyssiere, H. Beil, R. Bergere, P. Carlos, and A. Lepretre, Nucl. Phys. A159, 561 (1970).
[25]H. P. Morsch and P. Decowski (unpublished).
[26]M. Nagao and Y. Torizuka, Phys. Lett. 37B, 383 (1971).
[27]A. Scott, N. P. Marthur, and F. Petrovich, Nucl. Phys. A285, 222 (1977).
[28]G. R. Satchler, Part. Nucl. 2, 147 (1971).
[29]N. Marty, M. Morlet, A. Willis, V. Comparat, and R. Frascaria (unpublished).
[30]C. Süksd and H. P. Morsch (unpublished).